IEEE Access
Multidisciplinary | Rapid Review | Open Access Journal

Received December 24, 2020, accepted January 20, 2021, date of publication February 3, 2021, date of current version February 10, 2021.

Digital Object Identifier 10.1109/ACCESS.2021.3055867

Study for Influence of Harmonic Magnetic Fields on Vibration Properties of Core of Anode Saturable Reactor in HVDC Converter Valve System

YAQI WANG[1], CHONG GAO[2], LIN LI[1], (Member, IEEE), YUELEI FENG[1], AND YANG LIU[2]

[1]State Key Laboratory of Alternate Electrical Power System with Renewable Energy Sources, North China Electric Power University, Beijing 102206, China
[2]Global Energy Interconnection Research Institute, Beijing 102211, China

Corresponding author: Lin Li (lilin@ncepu.edu.cn)

This work was supported by the National Key Research and Development Program of China under Grant 2017YFB0903900 and the Science and Technology Project of State Grid Corporation of China under Grant 5455DW170024.

ABSTRACT The cores of anode saturated reactor (ASR) are the main vibration source of the HVDC converter valve system. The ASR is excited with an impulse voltage, which contains many harmonic components, and the magnetostriction of cores is usually the main reason of the ASR vibration. Therefore it is significant to study the influence of the harmonic on the vibration of core of ASR. In this paper, the magneto-mechanical coupling model is established based on the magnetostriction theory and the expression of vibration acceleration in the presence of third harmonic is derived. The vibration test platform is built to test the core's vibration acceleration. The magnetic and magnetostrictive properties of silicon steel sheet under different working conditions are measured. The three-dimensional simulation model of the core is established, and the vibration acceleration under different magnetic flux density is calculated. The comparison of the experiment and simulation results shows the rationality of the magneto-mechanical coupling model. The influence of third harmonic magnetic flux density on vibration is studied by changing the phase of the third harmonic magnetic flux density and the ratio of the third harmonic magnetic flux density to the fundamental magnetic flux density. Both the calculated and measured results show that the third harmonic magnetic flux density affects the vibration acceleration according to the double-frequency components of the third harmonic, as well the sum-frequency and difference-frequency components of the third harmonic and fundamental frequency.

INDEX TERMS HVDC, anode saturable reactor, magnetostriction, vibration, harmonic.

I. INTRODUCTION

HVDC technology has been developed in recent years, by converting the AC power into DC power at the sending end, and then transmitting to the receiving end, where the DC power is inverted into AC power to feed back to the AC system [1]–[5]. The anode saturated reactor (ASR) is the key component in the HVDC system. The vibration problem of ASR is very prominent, which mainly comes from the cores of ASR [6]. A model of ASR is shown in Figure.1. When the converter valves are turned on and turned off, the ASR endures a large impulse voltage, which contains a lot of harmonics, and the spectrum of the impulse voltage is shown in Figure.2. The harmonics current will aggravate the core vibration of the ASR [7]. The core vibration will in one hand cause the large noise, which destroys the working environment, and in another hand accelerate the device aging, reduce service life of the device, and even reduce the working life of the converter valve system [8].

Under the magnetic field provided by the winding current of ASR, the magnetic core is subject to Maxwell's electromagnetic force [9], [10]. At the same time, the length and

The associate editor coordinating the review of this manuscript and approving it for publication was Ahmad Elkhateb.

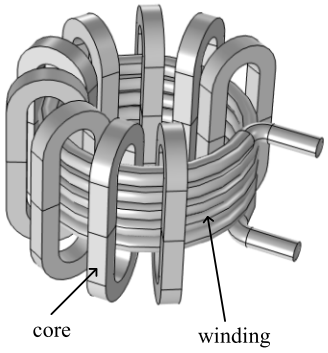

FIGURE 1. The model of ASR.

volume of ferromagnetic materials of core change slightly due to the core magnetization, which is called magnetostrictive effect and magnetostrictive force [11]–[13].

Chukwuchkwa *et al.* have studied how to reduce the magnetic core noise caused by magnetostrictive effect [14]. The vibration signal analysis method in power transformer monitoring has been extensively studied [15]–[17]. Many measurements have been made on the test transformers in the laboratory and in the manufacturing process of power transformers [18]–[23]. It is pointed out that magnetostriction of oriented electrical steel is the main source of vibration and noise of power transformer, which shows that the high magnetostriction is mainly due to the large transverse magnetic moment [24].

Like the power transformer core, the ASR cores are made of ultrathin silicon steel sheets. The magnetostrictive effect of the ultrathin silicon steel sheet under the action of alternating magnetic field and the electromagnetic force caused by magnetic flux leakage between the core laminations and joints are main reasons of vibration [25], [26]. With the improvement of manufacturing technology, the electromagnetic force caused by magnetic flux leakage between the core laminations and joints is far less than the magnetostrictive force, so the vibration induced by electromagnetic force can be ignored compared with the vibration induced by magnetostrictive effect [27]. The magnetostriction of the ultrathin silicon steel sheet is nonlinear with the magnetic field [28]. The anisotropy, applied stress, and temperature will have a great influence on the magnetostriction of silicon steel sheet [29]–[31].

The existing research on the core vibration of ASR is mainly carried out under sinusoidal excitation, but the actual excitation is impulse voltage containing multiple harmonics. Due to the existence of harmonics, the magnetic and magnetostrictive properties of silicon steel sheet will change greatly compared with that under sinusoidal excitation, which will lead the change of core vibration characteristics. Therefore, it is necessary to study the influence of harmonic on core vibration.

In this paper, the magneto-mechanical coupling model of the core of the ASR core is firstly established. Then three-dimensional simulation model of core is established to calculate the vibration acceleration. A core vibration test platform is built to test the ASR core's vibration. Finally, through changing the ratio of third harmonic magnetic flux density to the fundamental magnetic flux density and the phase of the third harmonic magnetic flux density, the influence of harmonics on the core vibration is studied.

II. METHODOLOGY

A. ELECTROMAGNETIC FIELD EQUATIONS

The ASR endures the large impulse voltage in practical operation, and the current contains a lot of harmonics which flows into the windings. The equation of magnetic field in the cores is as follows [32]:

$$\nabla \times \frac{1}{\mu}(\nabla \times \boldsymbol{A}) = \boldsymbol{J} - \sigma \frac{\partial \boldsymbol{A}}{\partial t} \tag{1}$$

where μ is the magnetic permeability (H/m). $\boldsymbol{A}$ is the magnetic vector potential, and the define of $\boldsymbol{A}$ is: $\boldsymbol{B} = \nabla \times \boldsymbol{A}$, where $\boldsymbol{B}$ is the magnetic flux density. $\boldsymbol{J}$ is the current density (A/m^2), and σ is the conductivity (S/m).

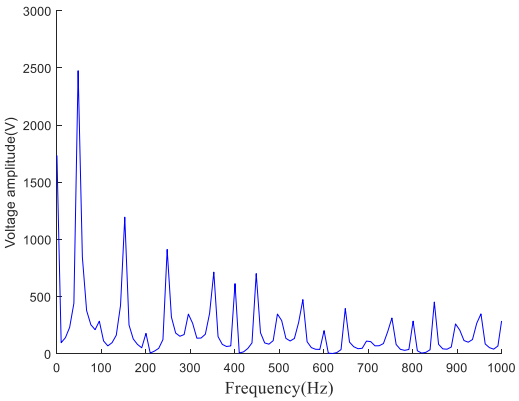

FIGURE 2. Frequency spectrum of impulse voltage.

B. MAGNETOSTRICTION PRINCIPLE

It can be seen from the Figure.2 that in the frequency spectrum of the excitation voltage of ASR, in addition to the basic component of 50 Hz, 150 Hz component accounts for the largest proportion. Therefore, the combination of fundamental and third harmonic components is taken as the main excitation to study the influence of harmonic on the vibration of core. Assume the expression of magnetic flux density is as follows:

$$B = B_1 cos\omega_1 t + B_3 cos\left(\omega_3 t + \theta\right) \tag{2}$$

where B_1 is the amplitude of fundamental magnetic flux density, B_3 is the amplitude of third harmonic magnetic flux density, $\omega_1 = 2\pi f$ is the fundamental angular frequency and f is the frequency of driving voltage, ω_3 is the third harmonic angular frequency, and θ is the phase of third harmonic magnetic flux density. The applied magnetic field intensity H

is [33]:

$$H = \frac{H_c}{B_S} B = \frac{H_c}{B_S} \left(B_1 cos\omega_1 t + kB_3 cos\left(\omega_3 t + \theta\right)\right) \quad (3)$$

where H_c is the coercive field intensity of material (A/m), and B_s is the saturation magnetic flux density (T).

The magnetostriction with driving magnetic-field H is the fraction change rate of the ultrathin silicon steel sheets around the direction of the winding length. The fraction change equation is [34]:

$$\frac{1}{L}\frac{dL}{dH} = \frac{2\lambda_s}{H_c^2}|H| \quad H \le H_c \quad (4)$$

where λ_s is the coefficient of saturation magnetostriction of the material, L is the length of material of rod geometry (m), and H_c is the coercive field intensity of material (A/m).

Integrating (4), the fractional change in length is obtained as:

$$\lambda = \frac{\Delta L}{L} = \frac{\lambda_s}{H_c^2} H^2 \quad (5)$$

Then, the core's vibration acceleration caused by magnetostriction is:

$$a = \frac{v}{t} = \frac{d^2\left(\Delta L\right)}{dt^2} \quad (6)$$

where a is the acceleration of core vibration. Combine with formula (3), (5), and (6), the acceleration of core can be described as:

$$\begin{aligned} a = -\frac{\lambda_s L}{B_s^2}\Big[&2\omega_1^2 B_1^2 cos2\omega_1 t + 2\omega_3^2 B_3^2 cos\left(2\omega_3 t + 2\theta\right) \\ &+ B_1 B_3 \left(\omega_1 + \omega_3\right)^2 cos\left(\omega_1 t + \omega_3 t + \theta\right) \\ &+ B_1 B_3 \left(\omega_1 - \omega_3\right)^2 cos\left(\omega_3 t - \omega_1 t + \theta\right) \end{aligned} \quad (7)$$

It can be seen from equation (7) that the vibration of the core includes the double frequency of the fundamental, the double frequency of the third harmonic, and the sum and difference frequency of the third harmonic and fundamental. So Reasonable control of the ratio of third harmonic and the phase of third harmonic can effectively reduce the core vibration.

For convenience, k is used to represent the ratio of the third harmonic magnetic flux density to the fundamental magnetic flux density, that is, $k = B_3/B_1$, and θ is used to represent the phase of the third harmonic magnetic flux density.

III. ANALYSIS OF MAGNETIC AND MAGNETOSTRICTIVE PROPERTIES OF SILICON STEEL SHEET UNDER HARMONIC EXCITATION

To accurately calculate the electromagnetic vibration of ASR core, the magnetic and magnetostrictive properties of silicon steel sheet under various magnetizing conditions should be measured and analyzed because the material under different types of magnetizing conditions shows different saturated nonlinearity.

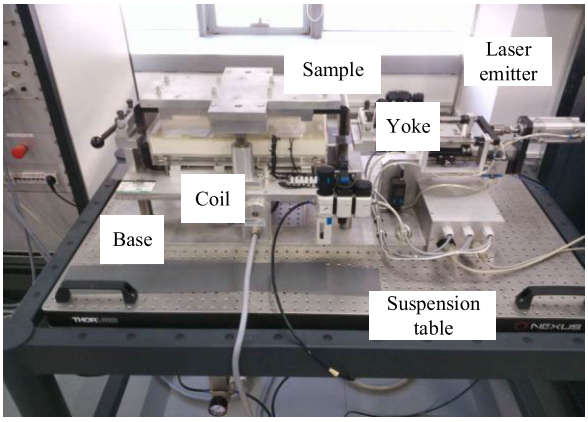

FIGURE 3. Magnetization and magnetostriction measurement device.

The measuring system is shown in Figure.3, which conforms to the standard IEC/TR62581. The measurement system consists of three parts: host, magnetic circuit device and laser transmitting and receiving device. In order to reduce the influence of the surrounding environment on the measurement results, the whole magnetic circuit device and laser transmitting and receiving device are placed on a suspension platform supported by air compressor. The magnetic circuit device consists of a group of excitation coils and a set of induction coils. The samples with effective length and width of 600mm and 100mm are placed in the inner cavity of the coil group. One end of the sample piece is fixed, and the other end can be freely retracted.

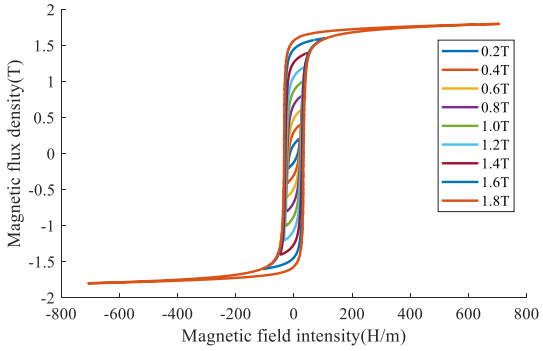

FIGURE 4. Hysteresis loop under 50Hz sinusoidal excitation.

The sample is applied 50Hz sinusoidal excitation, and the magnetic flux density is kept and tested from 0.1T to 1.8T in steps of 0.05T. The measured magnetic hysteresis loop is shown in Figure.4. It can be seen from the Figure.4 that when the magnetic flux density is less than 1.6T, the area of the hysteresis loop of the silicon steel sheet increases slowly with the increase of magnetic flux density. When the magnetic flux density is 1.8T, the area of the hysteresis loop is the largest and the silicon steel sheet is in saturated state.

Figure.5 shows the waveform of magnetic flux density under 1.2T in different k and θ. According to Figure. 5(a), when the excitation has no harmonic, the waveform of magnetic flux density is sinusoidal. With the appearance of

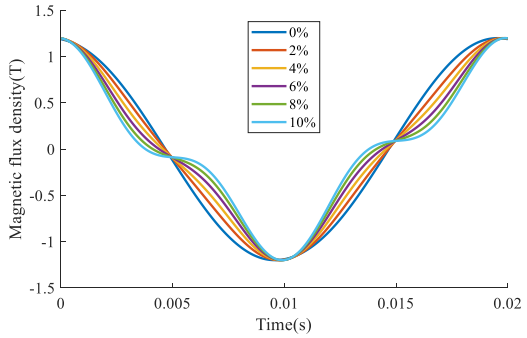

(a) Different k

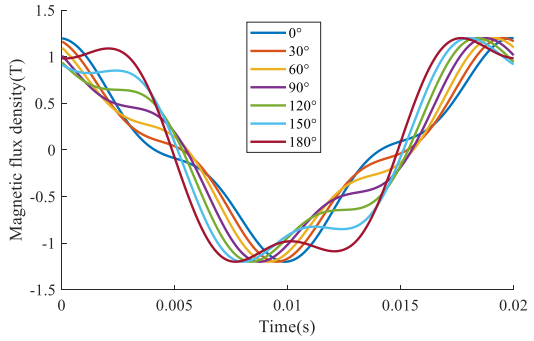

(b) Different θ

FIGURE 5. Waveforms of magnetic flux density.

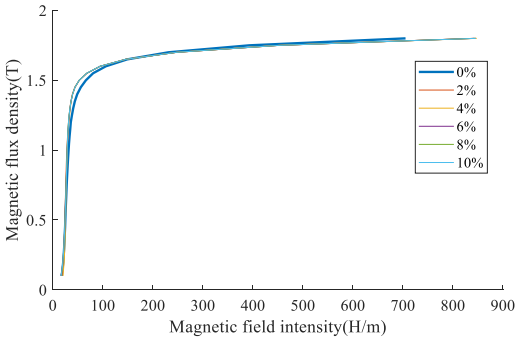

(a) Different k

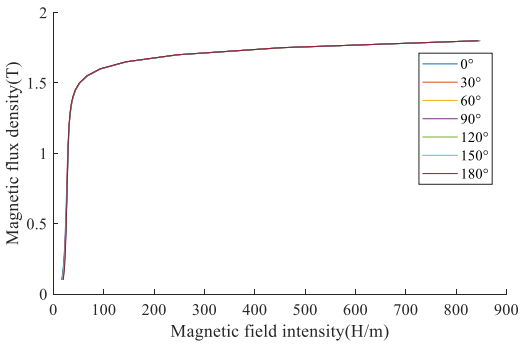

(b) Different θ

FIGURE 6. Magnetization curves.

harmonic in the excitation, the magnetic flux density appears distortion, and the distortion worsens with the increase of harmonic proportion. It can be seen from Fig. 5(b) that the distortion of the magnetic flux density waveform increases with the increase of θ.

The magnetization curves of silicon steel sheet under different k and θ are shown in the Figure.6, which are obtained by connecting the vertices of the hysteresis loops. It can be seen that the saturation magnetization of silicon steel sheet increases due to the existence of harmonic component in excitation, while the influence of different k and θ on the magnetization characteristics of silicon steel sheet can be almost ignored.

Figure 7(a) shows the magnetostriction butterfly curve of silicon steel sheet under 50 Hz sinusoidal excitation. It can be seen from the figure that the butterfly wings are symmetrical and the silicon steel sheet is in an elongated state. With the increase of magnetic flux density, the amplitude of magnetostrictive strain gradually increases and reaches the maximum value when the magnetic flux density is 1.8T. The time-domain curve of magnetostriction of silicon steel sheet in a period under different magnetic flux densities is shown in the Figure. 7(b). It can be seen that the magnetostriction of silicon steel sheet changes periodically. When the magnetic flux density reaches 1.6T, the waveform will be greatly distorted. Fourier analysis of the waveform is shown in Figure.7(c), which shows that when the magnetic flux density is below 1.6T, the magnetostriction is mainly concentrated at 100Hz and 200Hz. However, when the magnetic flux density is greater than 1.6T, the magnetostriction appears high order harmonics. This is because the magnetostriction is not only caused by the movement of the magnetic domain wall, but also related to the rotation of the magnetic domain.

In order to use the measured magnetostrictive data in FEM, the peak-to-peak value of magnetostriction λ_{pp} can be obtained from the difference between positive peak value (λ_{p+}) and negative peak value (λ_{p-}), thus a series of single value magnetostriction curves λ_{pp}-B_m under different k and θ can be depicted as shown in Figure.8. It can be seen that the single value curves of magnetostriction show obvious differences under different k and θ, especially in the saturation stage.

IV. SIMULATION AND EXPERIMENTAL SET UP

A. SIMULATION MODEL

A core of ASR is simulated by using the finite element simulation software. The simulation modules include magnetic field, circuit and solid mechanics. The mesh division of the core in the three-dimensional simulation model is shown in Figure.9. The iron core is clamped by an iron hoop, because there are two parts of the core. In order to simulate the effect of the iron hoop, the top and bottom of the core are set as fixed constraints. The turn number of excitation winding is 22, and the excitation winding is wrapped around the core limbs. In order to extract the vibration signal as complete as possible, the sampling frequency is 32 kHz.

In the simulation, the lamination coefficient, conductivity, relative permittivity, density, Poisson's ratio, Young's

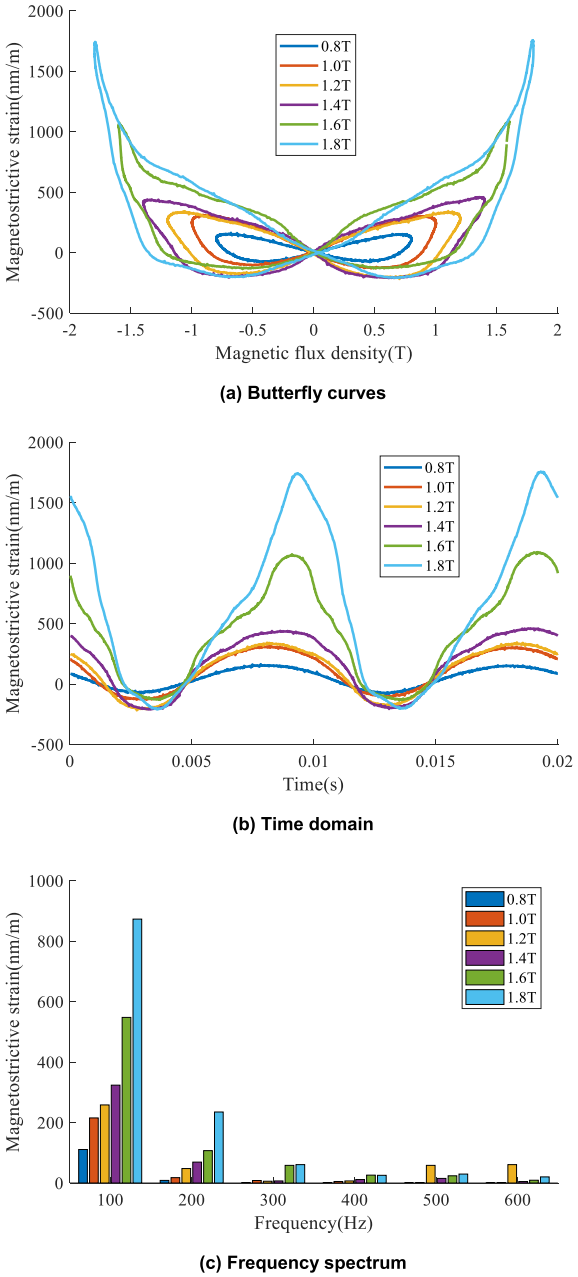

FIGURE 7. Magnetostriction under 50Hz sinusoidal excitation.

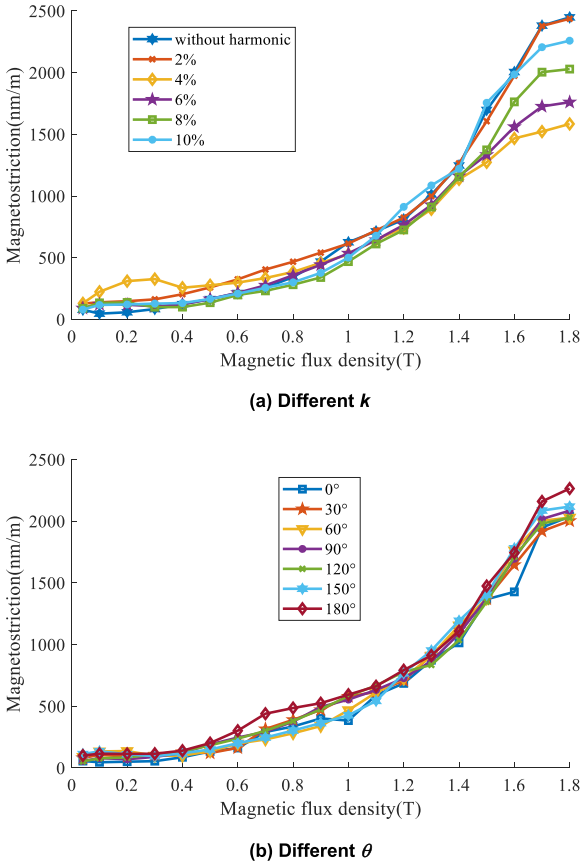

FIGURE 8. Magnetostrictive curve under different k and θ.

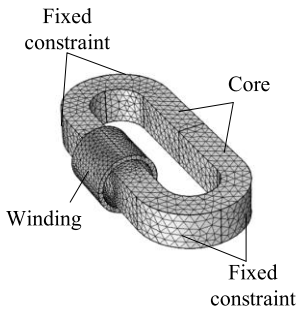

FIGURE 9. Simulation model of the core.

modulus, permeability, saturation magnetization and magnetostrictive constant are considered. Among them, conductivity, relative permittivity, density, Poisson's ratio and Young's modulus are obtained from the manufacturer, which can be directly set in the material properties in the simulation. The permeability, saturation magnetization and magnetostrictive constant are measured by the measuring equipment shown in Figure.3. The magnetization curve can be interpolated in the material properties, and the saturation magnetization and magnetostrictive constant are set in the globally defined parameters. As for lamination coefficient, the effective cross-sectional area of the core is equal to the actual cross-sectional area times the lamination coefficient.

B. EXPERIMENTAL SET UP

The measurement platform is shown in Figure.10. The Personal Computer 1 (PC1) control the programmable power supply to provide excitation for the winding. The turn number of winding are 22. The piezoelectric acceleration sensor is attached to the core by a magnetic base, and its sensitivity is 47.8mV/g. The data collector can get the real-time signal of acceleration and transmit it to the computer and the sampling frequency is 32 kHz. The Personal Computer 2 (PC2) is used to analyze and processes the signal. The core is placed on a sponge to reduce the effect of the ground on the core vibration.

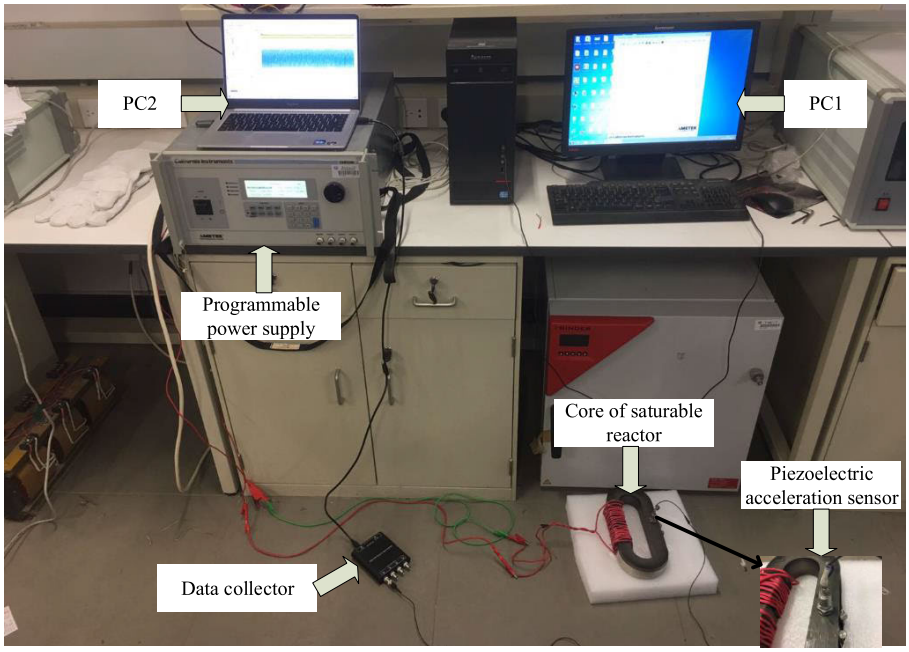

FIGURE 10. Vibration test platform.

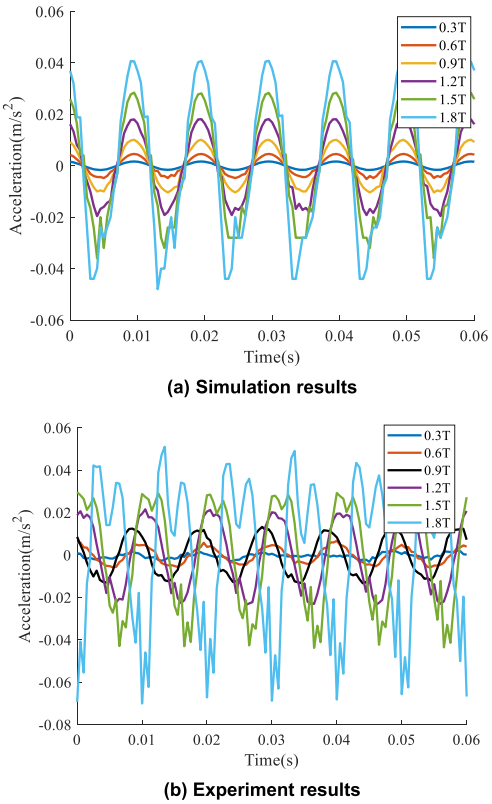

FIGURE 11. Time domain vibration acceleration.

V. RESULTS AND DISCUSSION

The simulation vibration acceleration of ASR core under different magnetic flux density is shown in the Figure. 11(a), and measured vibration acceleration of iron core under different magnetic flux density is shown in the Figure.11(b). It can be seen that both simulation acceleration and measured acceleration change periodically. With the increase of the magnetic flux density, the amplitude of the acceleration gets larger. The waveform of 0.3T, 0.6T and 0.9T are nearly close to sinusoidal wave. But when the magnetic flux density is 1.2T, the waveform has obvious distortion, and with the increase of the magnetic flux density, the distortion level gets heavier. The comparisons of time-domain simulation acceleration and test acceleration under 0.9T and 1.8T are shown in the Figure.12. It can be seen from Figure.12(a) that when the magnetic flux density is 0.9T, the acceleration amplitude of simulation and experiment are 0.01m/s^2 and 0.013m/s^2, respectively. The Figure. 12(b) shows that the acceleration amplitude of simulation and experiment are 0.041m/s^2 and 0.068m/s^2 with the magnetic flux density is 1.8T. To analyze the waveform more specifically, frequency spectrum diagrams of vibration acceleration with 0.9T and 1.8T are obtained through the FFT analysis, which is shown in Figure.13. From Figure.13(a), the acceleration frequency of both simulation and experiment results mainly concentrated in 100Hz, in which the simulation reaches 0.0098m/s^2 and the experiment reaches 0.0118m/s^2. At the same time, the acceleration frequency includes a small amount of 100Hz multiplications, and the multiplications can be almost ignored compared with the 100Hz component. Meanwhile, different from the Figure.13(a), the spectrum contains the frequency components 100Hz and a lot of its multiplications with the magnetic flux density is 1.8T, as shown in Figure.13 (b). The reason why this phenomenon occurs is that when the

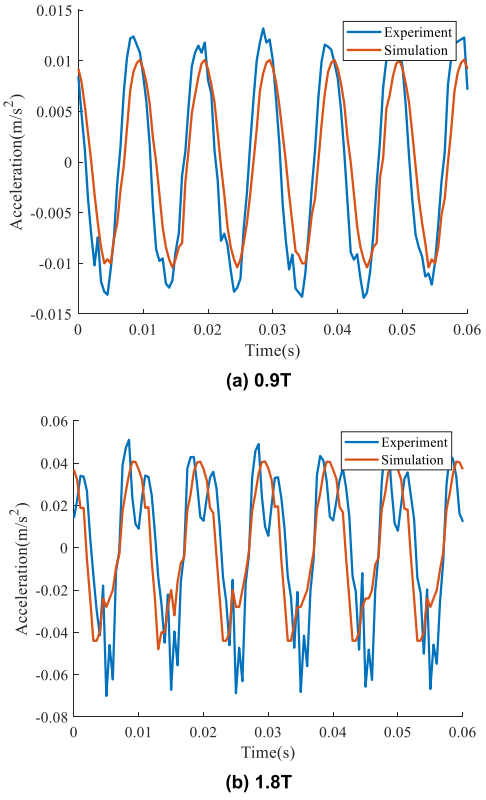

FIGURE 12. Comparison of time-domain accelerations calculated and measured.

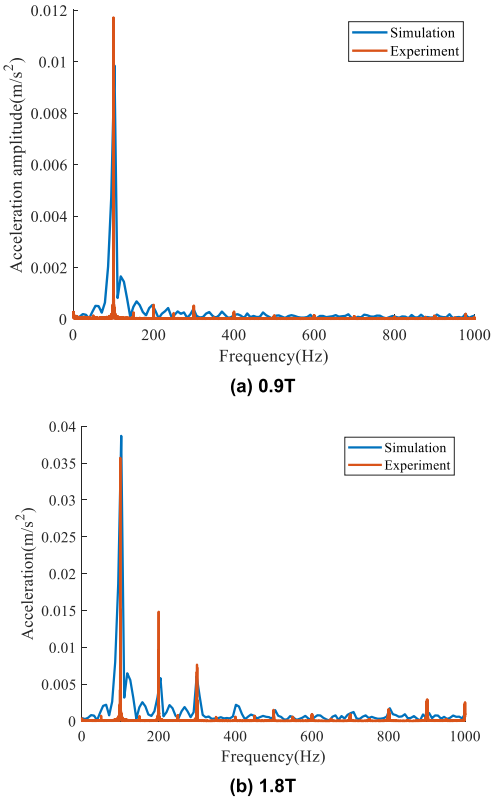

FIGURE 13. Comparison of spectrum accelerations calculated and measured.

magnetic flux density becomes saturated, magnetostriction is nonlinear with the magnetic field [35]. This is also why the waveform have distortion when the magnetic flux density comes to 1.2T and get larger.

Both the time-domain acceleration and spectrum acceleration show that there is a certain error between the simulation data and experiment data. The main reasons for the error between experiment and simulation are as follows: (1) The upper and lower surfaces of the core are set as fixed constraints in the simulation calculation, but the actual upper and lower bottom surfaces of the core are not completely fixed. (2) The young's modulus of the core is simplified to isotropy during the simulation. Generally speaking, the simulation results and the experimental results have the same change trend. At the same time, the error is also kept in the acceptable range, which verifies the correctness of the simulation.

In order to only study the influence of third harmonic magnetic flux density on the vibration of core, This article focuses on the vibration characteristics of the core when the flux density passing through the core is 0.9T, which is in the unsaturated stage and the influence of the nonlinear characteristics of magnetostriction can be ignored. In the process of measurement, the amplitude B of the magnetic flux density is 0.9T. The ratio k changes from 2% to 10%, with the interval of 2%. The phase θ changes from 0° to 180° and the interval is 30° and the phase of fundamental magnetic flux density remains 0°.

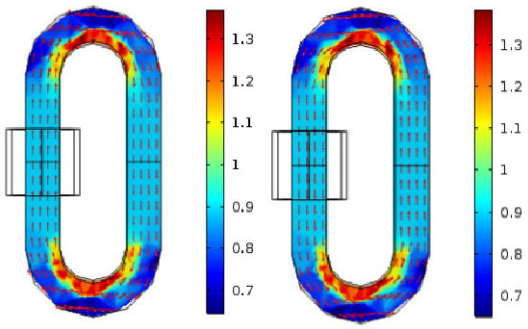

FIGURE 14. Magnetic flux density distributions under $B = 0.9$T, $B_3 = 8\%B_1$ and $\theta = 120°$ at 45ms and 55ms.

Figure.14 shows the magnetic flux density distribution under $B = 0.9$T, $B_3 = 8\%B_1$ and $\theta = 120°$ at 45ms and 55ms. It can be seen from the Figure.14 that in one period, the magnetic flux density changes obviously at different time, and at 45ms and 55ms, the excitation is positive and negative half cycle respectively, and the direction of magnetic flux density is opposite. The maximum and minimum values of magnetic flux density appear on the inside and outside of the core corner respectively. The flux density of the straight line part of the core is 0.9T, which is consistent with the theoretical calculation. Figure.15 shows the magnetostrictive stress distribution, and it can be seen that the maximum and minimum values of magnetostrictive stress correspond

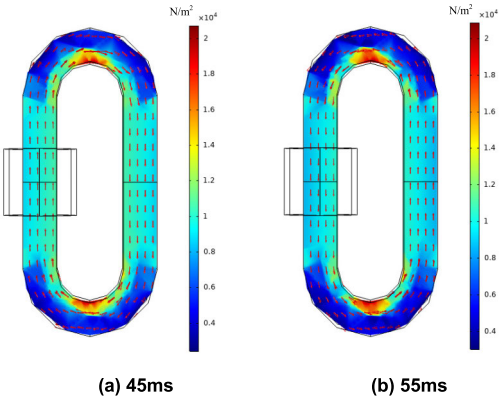

FIGURE 15. Magnetic force distribution under $B = 0.9$T, $B_3 = 8\%B_1$ and $\theta = 120°$ at 45ms and 55ms.

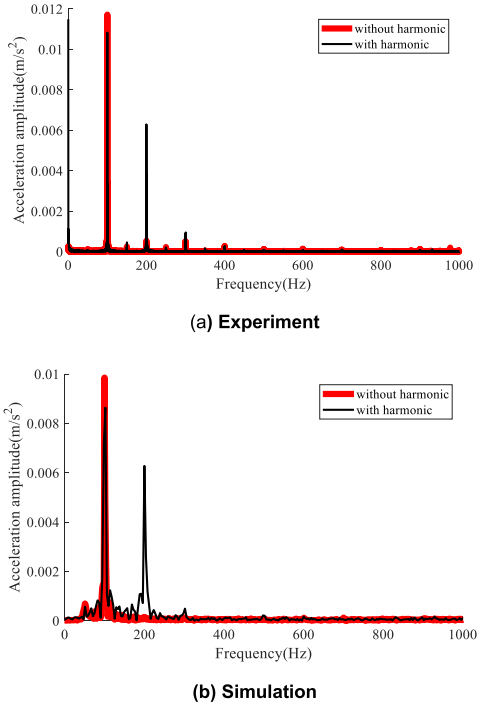

FIGURE 16. Comparison of the frequency spectrum of vibration acceleration without and with harmonic ($B = 0.9$T, $B_3 = 8\%B_1$ and $\theta = 120°$).

to the positions where the maximum and minimum values of magnetic flux density appear respectively.

Figure.16 shows the simulation and experiment of the frequency spectrum of vibration acceleration without and with harmonic($B = 0.9$T, $B_3 = 8\%B_1$ and $\theta = 120°$). In order to intuitively compare the vibration spectrum with and without harmonics, the simulation and experimental results are represented by different thickness and color. It can be seen from the Figure.16 that both simulation and experiment show that from no harmonic to including third harmonic, the changes are mainly concentrated in 100Hz, 200Hz and 300Hz. This is consistent with the meaning shown in equation (9). Therefore, this article mainly focus on the influence of third harmonic magnetic flux density on the vibration acceleration components of 100Hz, 200Hz and 300Hz.

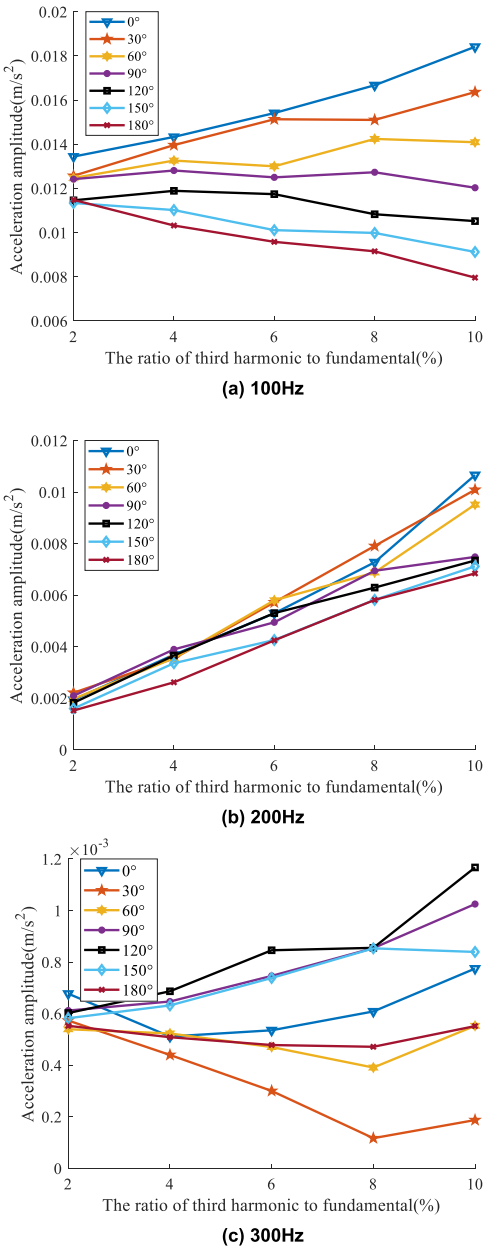

FIGURE 17. Vibration acceleration with different k.

Figure.17 shows the change of acceleration amplitude with k under different θ. It can be seen from the Figure.17(a) that with the increase of k, 100Hz component has an increase trend when the θ is less than 90°, an decrease trend when the θ is bigger than 90°, and remains nearly constant when the θ is 90°. Moreover, the larger the difference between θ and 90°, the more obvious the trend. Figure.17(b) shows that the component of 200Hz keeps the trend of increasing with k, no matter what the θ is. Figure.17(c) shows that 300Hz component of acceleration does not have obvious rule with k.

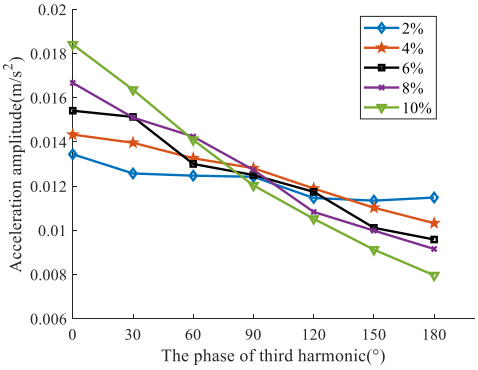

(a) 100Hz

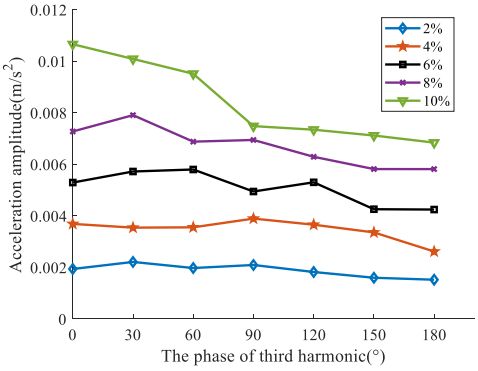

(b) 200Hz

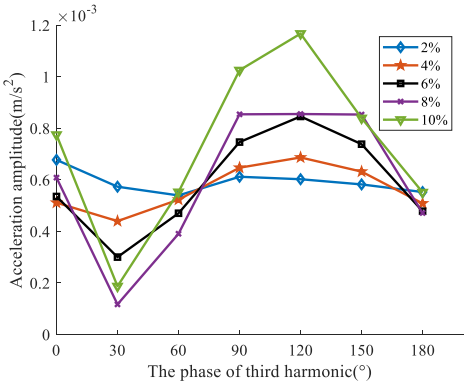

(c) 300Hz

FIGURE 18. Vibration acceleration with θ.

Figure.18 shows the change of acceleration amplitude with θ under different k. It can be seen from the Figure. 18(a) that 100Hz component of acceleration decreases with the increase of θ, and the decrease range get larger with k increases. Figure. 18(b) shows that the component of 200Hz has a small decrease in general, especially when $B_3 = 10\%B_1$, and as same with 100Hz component, its change range becomes larger with k increases. As for 300Hz component, it acts out the regular pattern of first decreasing, then increasing and finally decreasing. Moreover, like 100Hz and 200Hz component shown in Figure.18(a) and Figure.18(b), 300Hz component has the biggest change range when k is 10%, and the minimum when k is 2%.

VI. CONCLUSION

The magneto-mechanical coupling model is firstly established of the core of the anode saturable reactor in this paper. Then the magnetic and magnetostrictive properties of silicon steel sheet under different working conditions are measured. The correctness of the coupling model is verified by the comparison of simulation and measured results. Finally, the influence of harmonic on core vibration is studied by controlling different k and θ. Conclusions can be get by analyzing the frequency spectrum of vibration acceleration as follows:

(1) With the magnetic flux density increases, the vibration acceleration amplitude get larger, and its frequency spectrum mainly contains doubling of the fundamental, the frequency doubling of the harmonic, and the sum and difference frequency of the harmonic and fundamental. When the magnetic flux density is large enough to get saturation, the waveform has an obvious distortion, and frequency spectrum occurs higher harmonic, which can't be ignored.

(2) With k increases, the 100Hz component of vibration acceleration has an increase trend when the θ is less than 90°, and a decrease trend when the θ is bigger than 90°, and remains nearly constant when the θ is 90°. The component of 200Hz keeps the trend of increasing with the increase of k, no matter what the phase of third harmonic is. 300Hz does not have obvious rule.

(3) The increase of θ brings out the decrease of components of 100Hz and 200Hz, and 300Hz component presents that firstly decreases, then increases and finally decreases. All of them present that with k increases, the change range get larger.

REFERENCES

[1] X. Liang, P. Zhang, and Y. Chang, "Recent advances in high-voltage direct-current power transmission and its developing potential," *Power Syst. Technol.*, vol. 36, no. 4, pp. 1–9, Apr. 2012.

[2] J. Cao, F. Ji, J. Liu, and P. Chen, "Valve saturable reactor iron losses of ultrahigh-voltage direct current converter," *IET Sci., Meas. Technol.*, vol. 10, no. 2, pp. 77–83, Mar. 2016.

[3] J. Cao, C. Davidson, and S. Moulson, "Dynamic modelling of saturable reactor for HVDC applications," *IET Sci., Meas. Technol.*, vol. 1, no. 3, pp. 138–144, May 2007.

[4] Y. B. Shu, Z. H. Liu, L. Y. Gao, and S. W. Wang, "A preliminary exploration for design of ±800 kV UHVDC project with transmission capacity of 6400 MW," *Power Syst. Technol.*, vol. 30, no. 1, pp. 1–8, Jan. 2006.

[5] C. Liu, S. Hu, K. Han, Q. Hu, S. Gao, and W. Yao, "Electric-field distribution and insulation status of ±800kV UHVDC converter valve after implanting full-view micro-sensor detector," *IEEE Access*, vol. 7, pp. 86534–86544, 2019.

[6] P. Zhang, L. Li, J. Zhang, and C. Gao, "Vibration and noise reduction of HVDC anode saturable reactor by polyurethane damping elastomer," *Int. J. Appl. Electromagn. Mech.*, vol. 58, no. 2, pp. 261–273, Aug. 2018.

[7] S. Barg, K. Ammous, H. Mejbri, and A. Ammous, "An improved empirical formulation for magnetic core losses estimation under nonsinusoidal induction," *IEEE Trans. Power Electron.*, vol. 32, no. 3, pp. 2146–2154, Mar. 2017.

[8] M. Jin and J. Pan, "Effects of insulation paper ageing on the vibration characteristics of a transformer winding disk," *IEEE Trans. Dielectr. Electr. Insul.*, vol. 22, no. 6, pp. 3560–3566, Dec. 2015.

[9] J. Avila-Montes, D. Campos-Gaona, E. Melgoza Vazquez, and J. R. Rodriguez-Rodriguez, "A novel compensation scheme based on a virtual air gap variable reactor for AC voltage control," *IEEE Trans. Ind. Electron.*, vol. 61, no. 12, pp. 6547–6555, Dec. 2014.

[10] M. K. Ghosh, Y. Gao, H. Dozono, K. Muramatsu, W. Guan, J. Yuan, C. Tian, and B. Chen, "Proposal of Maxwell stress tensor for local force calculation in magnetic body," *IEEE Trans. Magn.*, vol. 54, no. 11, pp. 1–4, Nov. 2018.
[11] A. Lotfi and M. Faridi, "Design optimization of gapped-core shunt reactors," *IEEE Trans. Magn.*, vol. 48, no. 4, pp. 1673–1676, Apr. 2012.
[12] B. Tong, Y. Qingxin, Y. Rongge, Z. Lihua, and Z. Changgeng, "Research on stress characteristics of shunt reactor considering magnetization and magnetostrictive anisotropy," *IEEE Trans. Magn.*, vol. 54, no. 3, pp. 1–4, Mar. 2018.
[13] T. Tanzer, H. Pregartner, M. Riedenbauer, R. Labinsky, M. Witlatschil, A. Muetze, and K. Krischan, "Magnetostriction of electrical steel and its relation to the no-load noise of power transformers," *IEEE Trans. Ind. Appl.*, vol. 54, no. 5, pp. 4306–4314, Sep. 2018.
[14] N. Chukwuchekwa, A. J. Moses, and P. Anderson, "Study of the effects of surface coating on magnetic Barkhausen noise in grain-oriented electrical steel," *IEEE Trans. Magn.*, vol. 48, no. 4, pp. 1393–1395, Apr. 2012.
[15] C.-H. Hsu *et al.*, "Effects of magnetomechanical vibrations and bending stresses on three-phase three-leg transformers with amorphous cores," *J. Appl. Phys.*, vol. 111, no. 7, 2012, Art. no. 07E730.
[16] J. Shengchang, L. Yongfen, and L. Yanming, "Research on extraction technique of transformer core fundamental frequency vibration based on OLCM," *IEEE Trans. Power Del.*, vol. 21, no. 4, pp. 1981–1988, Oct. 2006.
[17] T. P. P. Phway and A. J. Moses, "Magnetisation-induced mechanical resonance in electrical steels," *J. Magn. Magn. Mater.*, vol. 316, no. 2, pp. 468–471, Sep. 2007.
[18] M. Rausch, M. Kaltenbacher, H. Landes, R. Lerch, J. Anger, J. Gerth, and P. Boss, "Combination of finite and boundary element methods in investigation and prediction of load-controlled noise of power transformers," *J. Sound Vib.*, vol. 250, no. 2, pp. 323–338, Feb. 2002.
[19] M. Mizokami, M. Yabumoto, and Y. Okazaki, "Vibration analysis of a 3-phase model transformer core," *Electr. Eng. Jpn.*, vol. 119, no. 1, pp. 1–8, Apr. 1997.
[20] B. Weiser, A. Hasenzagl, T. Booth, and H. Pfützner, "Mechanisms of noise generation of model transformer cores," *J. Magn. Magn. Mater.*, vol. 160, pp. 207–209, Jul. 1996.
[21] C. Bartoletti, M. Desiderio, D. DiCarlo, G. Fazio, F. Muzi, G. Sacerdoti, and F. Salvatori, "Vibro-acoustic techniques to diagnose power transformers," *IEEE Trans. Power Del.*, vol. 19, no. 1, pp. 221–229, Jan. 2004.
[22] B. Weiser, H. Pfutzner, and J. Anger, "Relevance of magnetostriction and forces for the generation of audible noise of transformer cores," *IEEE Trans. Magn.*, vol. 36, no. 5, pp. 3759–3777, Sep. 2000.
[23] B. García, J. C. Burgos, and M. Alonso, "Transformer tank vibration modeling as a method of detecting winding deformations—Part I: Theoretical foundation," *IEEE Trans. Power Del.*, vol. 21, no. 1, pp. 164–169, Jan. 2006.
[24] B. Weiser, A. Hasenzagl, T. Booth, and H. Pfützner, "Mechanisms of noise generation of model transformer cores," *J. Magn. Magn. Mater.*, vol. 160, pp. 207–209, Jul. 1996.
[25] A. Moses, "Measurement of magnetostriction and vibration with regard to transformer noise," *IEEE Trans. Magn.*, vol. 10, no. 2, pp. 154–156, Jun. 1974.
[26] B. Weiser, H. Pfutzner, and J. Anger, "Relevance of magnetostriction and forces for the generation of audible noise of transformer cores," *IEEE Trans. Magn.*, vol. 36, no. 5, pp. 3759–3777, Sep. 2000.
[27] P. Zhang, L. Li, Z. Cheng, C. Tian, and Y. Han, "Study on vibration of iron core of transformer and reactor based on maxwell stress and anisotropic magnetostriction," *IEEE Trans. Magn.*, vol. 55, no. 2, pp. 1–5, Feb. 2019.
[28] M. Yabumoto, S. Arai, R. Kawamata, M. Mizokami, and T. Kubota, "Recent development in grain-oriented electrical steel with low magnetostriction," *J. Mater. Eng. Perform.*, vol. 6, no. 6, pp. 713–721, Dec. 1997.
[29] A. Hasenzag, B. Weiser, and H. Pffitzner, "Magnetostriction of 3% Si Fe for 2-D magnetization patterns," *J. Magn. Magn. Mater.*, vol. 6, no. 160, pp. 55–56, 1996.
[30] S. Foster and E. Reiplinger, "Charcteristics and control of transformer sound," *IEEE Trans. Power App. Syst.*, vol. PAS-100, no. 3, pp. 1072–1077, Mar. 1981.
[31] P. Zhang and L. Li, "Vibration of saturable reactor core used in HVDC converter valve system," *J. Eng.*, vol. 2017, no. 14, pp. 2584–2590, Jan. 2017.
[32] M. Rausch, M. Kaltenbacher, H. Landes, R. Lerch, J. Anger, J. Gerth, and P. Boss, "Combination of finite and boundary element methods in investigation and prediction of load-controlled noise of power transformers," *J. Sound Vib.*, vol. 250, no. 2, pp. 323–338, Feb. 2002.
[33] B. X. Du and D. S. Liu, "Dynamic behavior of magnetostriction-induced vibration and noise of amorphous alloy cores," *IEEE Trans. Magn.*, vol. 51, no. 4, pp. 1–8, Apr. 2015.
[34] M. Weiner, "Magnetostrictive offset and noise in flux gate magnetometers," *IEEE Trans. Magn.*, vol. 5, no. 2, pp. 98–105, Jun. 1969.
[35] Y.-H. Chang, C.-H. Hsu, H.-L. Chu, and C.-P. Tseng, "Magnetomechanical vibrations of three-phase three-leg transformer with different amorphous-cored structures," *IEEE Trans. Magn.*, vol. 47, no. 10, pp. 2780–2783, Oct. 2011.

YAQI WANG was born in Hebei, China, in 1992. He received the B.E. degree from North China Electric Power University, Baoding, China, in 2016. He is currently pursuing the Ph.D. degree in electrical engineering with North China Electric Power University, Beijing, China.

His current research interest includes the vibration and noise of electric equipment.

CHONG GAO, photograph and biography not available at the time of submission.

LIN LI (Member, IEEE) received the B.Sc. and M.Sc. degrees in automation from the Hebei University of Technology, Tianjin, China, in 1984 and 1991, respectively, and the Ph.D. degree in electrical engineering from North China Electric Power University, Beijing, China, in 1997.

He is currently a Professor with the Department of Electrical and Electric Engineering, North China Electric Power University. His research interests include the theory and application of the electromagnetic field and electromagnetic compatibility of power systems.

YUELEI FENG was born in Hebei, China, in 1996. He received the B.E. degree from Chang'an University, Xi'an, China, in 2019. He is currently pursuing the master's degree in electrical engineering with North China Electric Power University, Beijing, China.

His current research interest includes the vibration and noise of electric equipment.

YANG LIU, photograph and biography not available at the time of submission.